Int. J. Heat Mass Transfer. Vol. 36, No. 8, pp. 2183–2192, 1993
Printed in Great Britain

0017-9310/93 $6.00+0.00

A theoretical investigation of acoustic enhancement of heat and mass transfer—I. Pure oscillating flow

MAN YEONG HA
Department of Mechanical & Production Engineering, The Pusan National University, 30 Jangjeon-Dong, Kumjung-Ku, Pusan 609-735, Korea

and

SAVASH YAVUZKURT
Department of Mechanical Engineering, The Pennsylvania State University, University Park, PA 16802, U.S.A.

(*Received* 25 *June* 1990 *and in final form* 7 *July* 1992)

Abstract—Effects of an oscillating flow induced by a high intensity acoustic field on heat and mass transfer to and from particles and droplets such as pulverized coal particles and coal–water slurry fuel droplets are investigated. Numerical solutions of two-dimensional, unsteady, laminar conservation equations for mass, momentum and energy transport in the gas phase give the velocity and temperature fields around a particle for different oscillating flows without superposed steady component as a function of time. The local and space-averaged Nusselt numbers depend on the change of imposed oscillating velocity U due to body curvature and flow acceleration. At low frequency (~ 50 Hz), curvature effects are dominant, resulting in increasing values of Nusselt numbers with increasing U. The Nusselt numbers can be approximated by the quasi-steady analysis. The effects of flow acceleration increase with increasing frequencies (~ 2000 Hz). The combined effects of curvature and flow acceleration result in the maximum difference of 9% in the space- and time-average Nusselt number for frequencies of 50, 1000 and 2000 Hz for the acoustic Reynolds number varying between 10 and 100. The present results show about 290% increase in the space- and time-averaged Nusselt number for an acoustic Reynolds number of about 100 compared to that without an acoustic field.

INTRODUCTION

THE EFFECT of an oscillating flow field with and without a steady component on heat and mass transfer from single spherical particles and droplets has been a topic of investigation since the late 1930s [1].

Baxi and Ramachandran [2] studied the effect of vibration on natural and forced convective heat transfer from spheres. In their experiments on free convection, a copper sphere was vibrated over the frequency range of 2.5–15.5 Hz for an amplitude range of 4–25 mm. For their forced convection experiments a frequency range of 3.3–26.7 Hz and amplitude range of 4–12 mm were used. The steady flow velocity varied between 7.5 and 25.6 m s^{-1}. The ratio of the acoustic (vibration) Reynolds number (Re_1) to the steady Reynolds number (Re_0) in the forced convection studies varied from 0 to 0.2. For free convective heat transfer, they observed increased heat transfer rates for $Re_1 > 200$. However, the vibration had no effect on the heat transfer rate in the forced convection studies for Re_1/Re_0 ratios of 0.0–0.2.

Mori *et al.* [3] studied the unsteady heat transfer from small spherical bodies (thermistors in the range of 0.245–1.46 mm diameter) and the evaporation rates of droplets in a sound field in parallel with a steady flow. The heat and mass transfer coefficients (Nusselt and Sherwood numbers) were obtained as a function of the acoustic Reynolds number based on time averaged velocities and the ratio of the unsteady and steady velocities (U_1/U_0) for low Strouhal numbers (0.00094–0.017). The frequency was varied over the range of 23–70 Hz and the maximum amplitude of the oscillating velocity was about 6 m s^{-1}, both in the presence and absence of a steady velocity component. The data were compared with theoretical predictions obtained assuming a quasi-steady flow based on the time averaged velocity of the oscillating flow with and without a steady component. Their results showed no dependence of the heat transfer rate on the Strouhal number for the low value (0.00094–0.017) used. Gibert and Angelino [4], in a similar experiment, derived an empirical relation for the mass transfer coefficient (Sherwood number) as a function of $(Re_1/Re_0)S^{0.45}$ in the ranges of $0.06 < (Re_1/Re_0)S^{0.45} < 0.60$, $1250 < Re_1 < 12\,000$ and $0 < Re_1/Re_0 < 2/\pi$ for frequencies of 0.76–3.64 Hz.

Larsen and Jensen [5] studied the evaporation rate of a single droplet of distilled water in a sound field from a loudspeaker transverse to the steady flow. The Reynolds number based on the oscillating velocity was varied over the range of 16–180 and Strouhal

NOMENCLATURE

D	diameter
f	frequency
h_θ	local heat transfer coefficient
i	static enthalpy
k	thermal conductivity
L_p	sound pressure level
Nu	Nusselt number
P	pressure
Pr	Prandtl number
r	radial position
R	radius of particle
R	gas constant, equation (6)
Re_1	acoustic Reynolds number ($U_1 D/\nu$)
S	Strouhal number
S_ϕ	source term for general variable ϕ
Sc	Schmidt number
Sh	Sherwood number
SPL	sound pressure level
t	time
T	temperature, period
u_r	radial velocity
u_θ	axial velocity
U_0	steady slip velocity
U_1	acoustic peak velocity.

Greek symbols

β	angular direction defined in the streamwise direction
γ	specific heat
Γ_ϕ	diffusivity for general variable ϕ
δ	boundary layer thickness
ε_ϕ	convergence criteria
ε	velocity ratio
θ	angular direction
μ	viscosity
ρ_g	gas density
τ	dimensionless time (tf or t/T)
ϕ	general variable given in Table 1
ω	angular frequency.

Subscripts

f	oscillating flow
g	gas
h	hydraulic
new	new values
old	old values
p	particle
r	radial
s	space-averaged, surface, separation
t	space- and time-averaged
0	initial
1	acoustic
θ	angular
ϕ	dependent variables
∞	infinity.

number was varied in the range of 0.3–2.8 with frequencies of 82–734 Hz and sound pressure levels of 132–152 dB. The steady convective Reynolds number was in the range of 5–45. The maximum increase in the Sherwood number for this range of parameters was about 90%.

Rawson [6], in his experiments on a vertical sonic water spray evaporator, achieved an average of 30% increase in the water evaporation rate in the presence of a high intensity acoustic field with a sound pressure level of 152 dB over the frequency range of 1100–1300 Hz.

All of these studies are related to unsteady heat and mass transfer over a single solid particle, droplet or droplets in the presence of an oscillating acoustic field with and without a steady convective velocity component for various frequency ranges. These results show an increase, decrease or unnoticeable change in heat and mass transfer, depending on the frequency and the magnitude of the steady and oscillating flow. As can be seen, the previous studies are generally concentrated on experimental aspects showing the global effect of oscillating flow field on heat and mass transfer. Due to the complexity of these problems, there are no detailed theoretical studies investigating the fundamental aspects of this problem in order to understand the governing mechanisms. The objective of this research is to emphasize fundamental aspects in order to investigate the effects of acoustic fields on heat and mass transfer to and from solid and droplet fuels such as pulverized coal and coal–water slurry fuels (with low particle density) which are entrained in the bulk gas flow for a significant period of time during the later stages of pulverized coal or coal–water slurry fuel (CWSF) combustion. This study is fundamental but at the same time it is comprehensive. This goal is achieved via the numerical solutions of the two-dimensional laminar, unsteady forms of the conservation of mass, momentum and energy for a spherical particle exposed to an oscillating acoustic velocity, $U_1 \cos(2\pi t/T)$. The effects of varying acoustic Reynolds number and Strouhal number on heat and mass transfer to and from single particle are investigated.

GOVERNING EQUATIONS AND BOUNDARY CONDITIONS

The hydrodynamic and thermal characteristics of an oscillating flow created by an acoustic field over a single particle are studied by solving the unsteady and two-dimensional axisymmetric conservation equa-

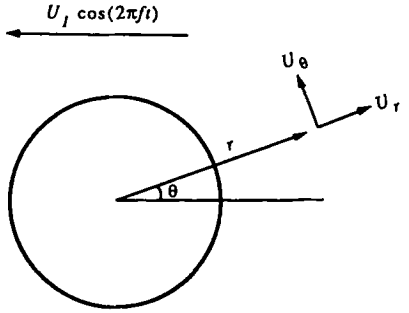

FIG. 1. Schematic diagram showing the geometry and some of the nomenclature used to simulate heat and mass transfer from a spherical particle in the presence of a high intensity acoustic field.

tions for constant property, laminar flow with the following common form (see Patankar [7]):

$$\frac{\partial}{\partial t}(\rho\phi)+\frac{1}{r^2}\frac{\partial}{\partial r}(r^2\rho u_r\phi)+\frac{1}{r\sin\theta}\frac{\partial}{\partial\theta}(\sin\theta\rho u_\theta\phi)=\frac{1}{r^2}\frac{\partial}{\partial r}\left(\Gamma_\phi r^2\frac{\partial\phi}{\partial r}\right)+\frac{1}{r^2\sin\theta}\frac{\partial}{\partial\theta}\left(\Gamma_\phi\sin\theta\frac{\partial\phi}{\partial\theta}\right)+S_\phi. \quad (1)$$

The flow field and the particle geometry with some nomenclature are shown in Fig. 1. In the conservation of momentum equation, $\phi = u_r$, u_θ represents the velocities in the radial r and axial θ directions, respectively. In the energy equation $\phi = i$ is the static enthalpy. The source terms S_ϕ in equation (1) are given in Table 1. The quantities are allowed to vary in the radial (r) and axial (θ) directions whereas a circumferential symmetry is assumed around an axis which passes through the center of the particle and is parallel to the flow direction.

The governing equation (1) has the following initial and boundary conditions:

Initial conditions ($t = 0$):

$$\phi = \phi_0 \quad (2)$$

Boundary conditions ($t > 0$):

$$\frac{\partial\phi}{\partial\theta} = 0, \quad \text{at } \theta = 0 \text{ and } \pi \text{ (Symmetry conditions)} \quad (3)$$

$$\phi = \phi_p, \quad \text{at } r = R \quad (4)$$

and as $r \to \infty$,

$$u_\theta = -U_1\cos(2\pi t/T)\sin\theta$$

$$u_r = U_1\cos(2\pi t/T)\cos\theta$$

$$i = i_\infty. \quad (5)$$

In equations (4) and (5), ϕ_p represents the value of the dependent variable ϕ at the particle surface and U_1 is the peak value of the acoustic velocity as defined by:

$$U_1 = \frac{\sqrt{2}\,10^{L_p-94/20}}{\rho_g(\gamma RT_g)^{0.5}} \quad (6)$$

where L_p represents the sound pressure level with the unit of dB.

In the present simulation of heat and mass transfer without chemical reactions, it is assumed that the species and energy conservation equations are decoupled, and therefore the solution of the energy equation with its boundary conditions in the proper dimensionless form also represents a solution to the species transport equation. This means that the present solution for heat and mass transfer is correct for the case of low heat and mass transfer as shown in ref. [8].

The velocities $u_{\theta p}$ and u_{rp} in equation (4) at the particle surface are zero. The static enthalpy i_p is a constant value determined by a specified particle temperature.

The numerical solutions of equation (1) using the above initial and boundary conditions give the velocity and temperature fields for oscillating flow over a spherical particle as a function of time. From the calculated temperature distribution, the local Nusselt number, Nu_θ, is calculated as

Table 1. Source terms S_ϕ used in equation (1)

ϕ	Γ_ϕ	S_ϕ
1	0	0
u_r	μ	$-\frac{\partial p}{\partial r}+\frac{1}{r^2}\frac{\partial}{\partial r}\left(\mu r^2\frac{\partial u_r}{\partial r}\right)+\frac{1}{r\sin\theta}\frac{\partial}{\partial\theta}\left(\mu\sin\theta\frac{\partial u_\theta}{\partial r}\right)-\frac{1}{r^2\sin\theta}\frac{\partial}{\partial\theta}(\mu\sin\theta u_\theta)-\frac{2\mu}{r^2}\frac{\partial u_\theta}{\partial\theta}-4\mu\frac{u_r}{r^2}-2\mu\frac{u_\theta\cot\theta}{r^2}+\rho\frac{u_\theta}{r^2}$
u_θ	μ	$-\frac{1}{r}\frac{\partial p}{\partial\theta}+\frac{1}{r^2}\frac{\partial}{\partial r}\left(\mu r^2\frac{\partial u_\theta}{\partial r}\right)+\frac{1}{r^2\sin\theta}\frac{\partial}{\partial\theta}\left(\mu\sin\theta\frac{\partial u_\theta}{\partial\theta}\right)+\frac{2}{r\sin\theta}\frac{\partial}{\partial\theta}\left(\mu\sin\theta\frac{u_r}{r}\right)+\frac{\mu}{r}\frac{\partial u_\theta}{\partial r}+\frac{\mu}{r^2}\frac{\partial u_r}{\partial\theta}-\mu\frac{u_\theta}{r^2}-2\mu\frac{u_r\cot\theta}{r^2}-2\mu\frac{u_\theta\cot^2\theta}{r^2}-\frac{1}{r^2}\frac{\partial}{\partial r}(\mu r u_\theta)-\rho\frac{u_r u_\theta}{r^2}$
i	k/c_p	0

$$Nu_\theta = \frac{h_\theta D}{k} = \frac{D}{(T_p - T_\infty)} \left.\frac{\partial T}{\partial r}\right|_{r=R}. \quad (7)$$

Integrating the local Nusselt number in the axial direction, the space-averaged Nusselt number denoted by Nu_θ is obtained. This is given by the following equation:

$$Nu_\theta = \frac{1}{\pi}\int_0^\pi Nu_\theta \, d\theta. \quad (8)$$

After the steady periodic state is reached, meaning that the space-averaged Nusselt number over a cycle is the same as the value obtained in the following cycles, the space- and time-averaged, quasi-steady Nusselt number, Nu_t, is calculated as follows:

$$Nu_t = \frac{1}{T}\int_0^T Nu_\theta \, dt \quad (9)$$

where T represents the period of the applied acoustic field. The important nondimensional parameters in the calculation of the space- and time-averaged, quasi-steady heat and mass transfer coefficients (Nu_t or Sh_t) without chemical reactions are:

Re_0: Reynolds number based on steady slip velocity U_0
$Pr(Sc)$: Prandtl (or Schmidt) number
$S(=fD/U_1)$: Strouhal number.

RESULTS AND DISCUSSION

In the present simulation of heat and mass transfer to and from a single spherical particle, the fluid is air with a free stream temperature of 20°C. The particle temperature is taken to be 40°C. The thermophysical properties such as viscosity, thermal conductivity, specific heat, etc. are calculated at a film temperature of 30°C since the property variation is small for the small temperature variation between 20°C and 40°C. The particle diameter is fixed at 100 μm in order to consider heat and mass transfer to and from small spherical particles such as pulverized coal particles and coal–water slurry droplets. The numerical solution domain is chosen to be 20 times the particle diameter with 30 grid points in the θ, and 50 in the r direction. The amplitude of the oscillating velocity (U_1) and the frequency (f) of the applied acoustic field are varied in order to obtain the values of the Nusselt and Sherwood numbers for different acoustic Reynolds and Strouhal numbers. One period or cycle is divided into 40 uniform time intervals, so that $\delta t = 1/40f$ is used as a numerical time step. A value of 0.005 is used for ε_ϕ in following equation (10) as a convergence criterion in the present simulation.

$$\varepsilon_\phi = \sum \left|\frac{\phi_{new} - \phi_{old}}{\phi_{new}}\right| \quad (10)$$

where ϕ_{old} represents the values of the previous iteration and ϕ_{new} the updated values from the present iteration for u_r, u_θ and i. The present numerical solution technique for equation (1) is the SIMPLEC algorithm of Van Doormaal and Raithby [9].

The separation angle and Nusselt number obtained from the present simulation agree well with previously published numerical and experimental results in refs. [3, 10–14] for the steady Reynolds number range of 10 to 100 (without a superposed oscillating velocity, $Re_1 = 0$), as shown by Ha [15]. These comparisons show that the present code is adequate for predicting the steady flow field and heat transfer for a spherical particle.

After the successful benchmarks made with steady flows, the program was run for the case of an oscillating flow (without a steady component) around a stationary spherical particle. In order to investigate the effects of the acoustic Reynolds number, the sound pressure levels varied in the range of 151–167 dB, resulting in the acoustic Reynolds number (Re_1) in the range 15.7–94.4, corresponding to U_1 values of 2.5–15 m s^{-1}. The frequencies used are 50, 1000 and 2000 Hz in order to study the effects of the Strouhal number, S, which lies in the range 0.00033–0.08. These sound pressure levels and frequencies are chosen in order to cover the range of conditions of previous experimental studies in refs. [2–6] investigating heat and mass transfer to and from particles or droplets in the presence of an oscillating flow. The detailed discussion on the flow fields, flow separation, axial pressure gradient and shear stress along the surface are shown by Ha [15].

For the small values of the Strouhal number, the velocity and temperature field reaches a steady periodic state after an early cycle. Thus the following discussion concentrates on the results over one cycle after reaching a steady periodic state, unless it is mentioned otherwise.

Figures 2 and 3 show the constant temperature lines in the domain from R to $8R$ for $Re_0 = 0.0$ and $Re_1 = 15.7$ ($U_1 = 2.5$ m s^{-1}) corresponding to $S = 0.002$ ($f = 50$ Hz) and $S = 0.08$ ($f = 2000$ Hz) over one cycle between $\tau = 0.0$ and 1.0. The constant temperature lines shown in Figs. 2 and 3 represent $(T - T_\infty)/(T_p - T_\infty)$ where T_p and T_∞ represent the temperatures at the particle surface and at infinity. At $\tau = 0.0$, the flow direction is from left to right and high temperature gradients are observed around the leading half of the sphere from $\theta = 180$ to 90, particularly near the stagnation point ($\theta = 180$). When the flow direction is reversed, the stagnation point is located at $\theta = 0$ and the location of higher temperature gradient is reversed. The difference in temperature fields encountered in these cases (50 and 2000 Hz) will be discussed later.

Figure 4 shows the local Nusselt number variation with angle with no steady flow corresponding to $S = 0.002$ ($f = 50$ Hz) and $S = 0.08$ ($f = 2000$ Hz) over the half cycle from $\tau = 0.0$ to 0.5. The Nusselt number is plotted as $Nu_\theta - 2$ to separate effects of pure conduction from convection. $Nu_\theta = 2$ corresponds to

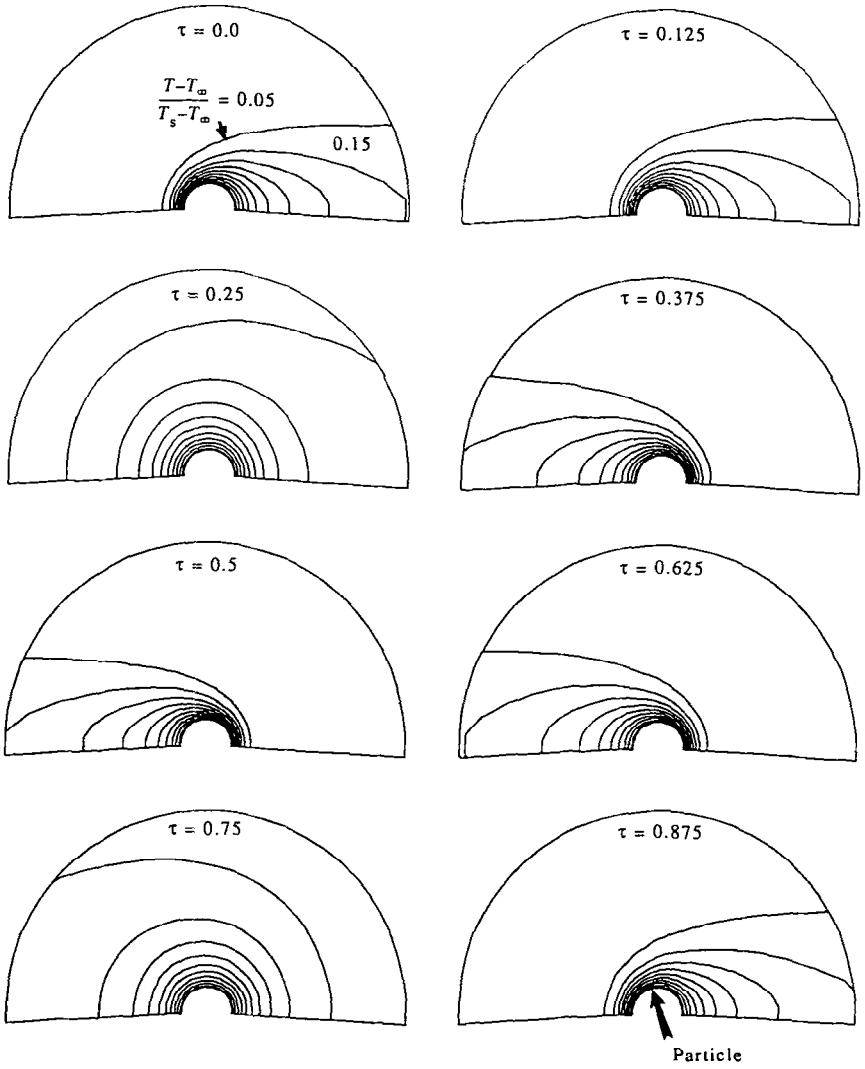

FIG. 2. Constant temperature lines due to an acoustic field with $SPL = 151$ dB and $f = 50$ Hz around a spherical particle of diameter 100 μm at different times during one cycle: $Re_\omega = 0.0$ (no steady flow), $Re_1 = 15.7$, $S = 0.002$.

a pure conduction value. Large variations with time in the local Nusselt number at $\theta = 0$ and 180 are observed compared with the variation at $\theta = 90$, as a consequence of the applied acoustic field.

As can be seen in Fig. 4, the maximum Nusselt number is observed at the stagnation point ($\theta = 180$ during $\tau = 0.0$–0.25). The maximum values of the Nusselt number at $\theta = 180$ and $\tau = 0$ are about 5.287 and 4.535 at frequencies of 50 and 2000 Hz, respectively. During the quarter cycle from $\tau = 0.0$ to 0.25, the maximum value of the Nusselt number decreases from 5.287 at $\tau = 0.0$ to 2.436 at $\tau = 0.25$ for the low frequency of 50 Hz and from 4.535 at $\tau = 0.0$ to 3.183 at $\tau = 0.25$ at the high frequency of 2000 Hz, as shown in Fig. 4, with decreasing oscillating acoustic velocity U.

The direction of the flow changes from right to left during the quarter cycle from $\tau = 0.25$ to 0.5. As a result, the stagnation point is located at $\theta = 0$. The Nusselt number at $\theta = 0$ and $\tau = 0.5$ is 5.536 at 50 Hz and 4.551 at 2000 Hz, which are higher than the values of 5.287 at 50 Hz and 4.535 at 2000 Hz at $\theta = 180$ and $\tau = 0.0$. It was noted by Tseng and Lin [16] that the values of the space-averaged Nusselt number corresponding to the negative maximum velocity are higher than those corresponding to the positive maximum velocity. As shown in refs. [17, 18] a small steady motion (acoustic streaming) is generated over a spherical particle in the presence of an acoustic field. Thus, it is expected that the phase lag between the applied acoustic field and the thermal boundary layer, and the steady streaming results in the differences in the Nusselt number at the stagnation points at $\tau = 0.0$ and 0.5.

The distribution of $Nu_\theta - 2$ at a dimensionless time from $\tau = 0.5$ to 0.75 is very similar to that from $\tau = 0.0$

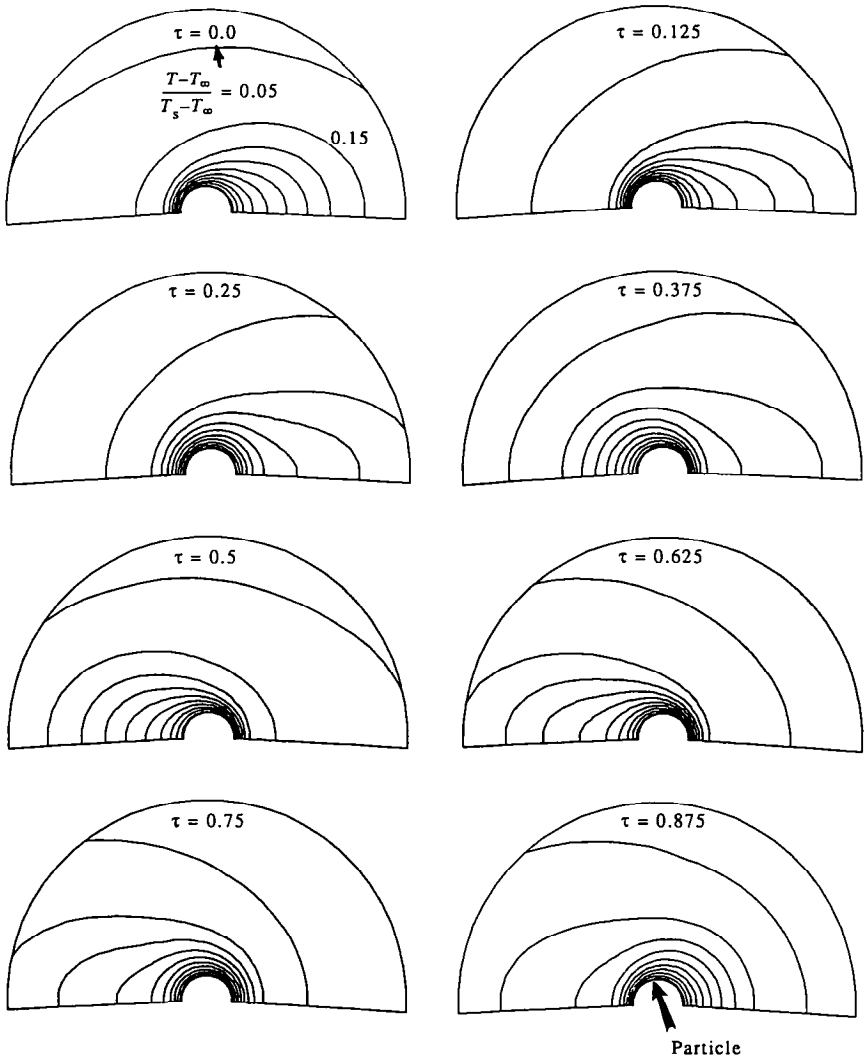

FIG. 3. Constant temperature lines due to an acoustic field with $SPL = 151$ dB and $f = 2000$ Hz around a spherical particle of diameter 100 μm at different times during one cycle $Re_0 = 0.0$ (no steady flow), $Re_1 = 15.7$, $S = 0.08$.

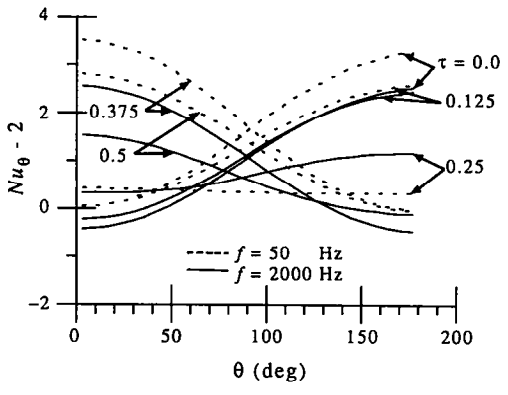

FIG. 4. Angular variation of local Nusselt number due to an acoustic field with $SPL = 151$ dB for frequencies of 50 Hz ($S = 0.002$) and 2000 Hz ($S = 0.08$) around a spherical particle of diameter 100 μm at different times during a half cycle from $\tau = 0.0$ to 0.5: $Re_0 = 0.0$ (no steady flow), $Re_1 = 15.7$.

to 0.25, and that at a dimensionless time from 0.75 to 1.0 is very similar to that from $\tau = 0.25$ to 0.5 except that they are anti-symmetric. There are minor differences due to the steady acoustic streaming over a spherical particle.

The characteristic time scale of the oscillating flow, $t_{ch,f}$, can be represented by $1/\omega$ where ω is an angular frequency. The magnitude of $t_{ch,f}$ is about 3.18 and 0.08 ms for frequencies of 50 and 2000 Hz, respectively. The characteristic time scale for momentum transport and heat transfer, $t_{ch,h}$ and $t_{ch,T}$, can be represented by δ_h (or δ_T)$/U_{rms}$ for the case of oscillating flow without a steady component where δ_h and δ_T represent, respectively, the hydraulic and thermal boundary layer thicknesses and U_{rms} represents the root-mean-square value of the oscillating flow velocity. Since the Prandtl number of the gas is about one, the magnitude of δ_h is almost the same as that of δ_T. If $t_{ch,T} \ll t_{ch,f}$, there is no time delay between the

thermal response and the applied acoustic field. In this case the space-averaged Nusselt number Nu_s can be well approximated by quasi-steady convection with an instantaneous velocity $U = |U_1(\cos 2\pi\tau)|$. Substituting this velocity U in place of U_0 in Re_0 in the correlation for the steady Nusselt number (for example, $Nu_0 - 2 = 0.6Re_0^{1/2} Pr^{1/3}$) yields the instantaneous space-averaged Nusselt number, Nu_s, corresponding to the velocity U. However, if $t_{ch,f} \ll t_{ch,T}$, the thermal boundary layer cannot follow the acoustic field. The time delay between the acoustic field and the thermal boundary layer will increase with increasing frequency. As a result the amplitude of the space-averaged Nusselt number, Nu_s, will decrease. This means that the high peak values of Nu_s will decrease but the low peak values of Nu_s will increase.

It is expected that the characteristic time of the response of the thermal layer does not heavily depend on the frequency but on Reynolds number. Since this response time is governed by the inertial and viscous forces, increasing Reynolds numbers decrease the response time. On the contrary, the characteristic time for the external flow depends on frequency not on Reynolds number. As mentioned earlier the ratios of these characteristic times control the process of heat and mass transfer. This discussion is supported by the following analysis. In order to calculate the approximate characteristic time scale for heat transfer, the thickness of the layer δ_T is defined at $\theta = 90$ by the location where the dimensionless temperature for $(T - T_\infty)/(T_p - T_\infty)$ is equal to 0.01. At the low frequency of 50 Hz, the magnitude of $t_{ch,T}$ at $\tau = 0.0$, 0.25 and 0.5 is about 0.046, 0.13 and 0.043 ms, respectively. These values for $t_{ch,T}$ are very small compared to 3.18 ms for $t_{ch,f}$. If the frequency is increased to 2000 Hz, the magnitude of $t_{ch,T}$ is 0.171 ms at $\tau = 0.0$, 0.157 ms at 0.25 and 0.165 ms at 0.50 which are larger than 0.079 ms for $t_{ch,f}$. As shown in Fig. 4, at $\tau = 0.0$ when the magnitude of the oscillating velocity U is at a maximum, the Nusselt number at 50 Hz is higher than that at 2000 Hz. But at $\tau = 0.25$ with a minimum value of the oscillating velocity ($U = 0$), the Nusselt number at 50 Hz is lower than that at 2000 Hz. The major reason for the difference observed at $\tau = 0.0$ is the phase lag between the acoustic field and the thermal boundary layer, caused by the difference of the time scales. However, as shown by Ha [15], during $\tau = 0.0$–0.25, flow separation is observed in the downstream region due to flow acceleration at 2000 Hz, resulting in the increase in the size of the wake. Here, the effect of flow separation due to flow acceleration is one major factor for the higher Nusselt number at 2000 Hz compared to the one at 50 Hz, in addition to the time delay.

When the acoustic Reynolds number is increased from 15.7 to 94.4, the boundary layer thickness is decreased, resulting in an enhanced heat transfer rate due to a steeper temperature gradient on the particle surface. The constant temperature lines for $Re_0 = 0.0$ and $Re_1 = 94.4$ with $S = 0.002$ ($f = 50$ Hz) and

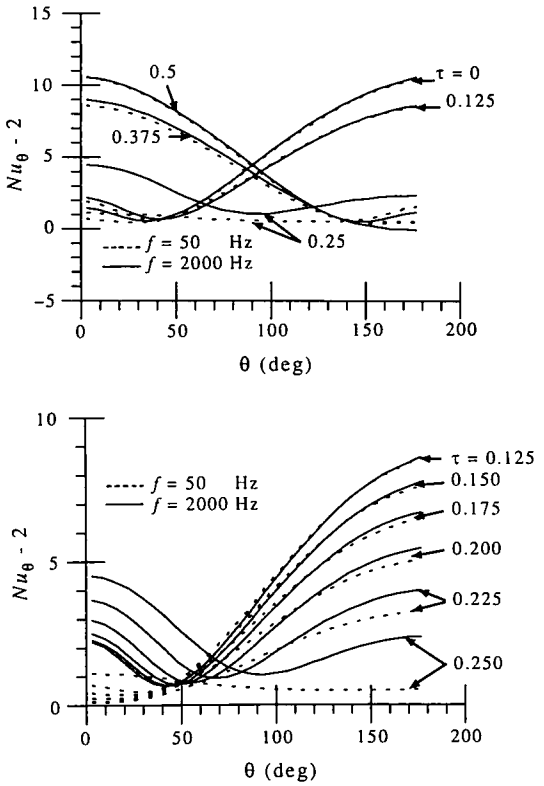

FIG. 5. Angular variation of local Nusselt number due to an acoustic field with $SPL = 167$ dB for frequencies of 50 Hz ($S = 0.00033$) and 2000 Hz ($S = 0.0013$) around a spherical particle of diameter 100 μm at different times during a half cycle from $\tau = 0.0$ to 0.5: $Re_0 = 0.0$ (no steady flow), $Re_1 = 94.4$.

$S = 0.08$ ($f = 2000$ Hz) are shown by Ha [15]. At 50 Hz, the values of $t_{ch,T}$ at $\tau = 0.0$, 0.25 and 0.5 are about 0.0043, 0.0186 and 0.0042 ms, respectively, which are very small compared to 3.18 ms for $t_{ch,f}$. When the frequency is increased to 2000 Hz, the values of $t_{ch,T}$ at $\tau = 0.0$, 0.25 and 0.5 are 0.0127, 0.0132 and 0.0127 ms, smaller than 0.079 ms for $t_{ch,f}$. Therefore, the Nusselt number at 2000 Hz is almost the same as that at 50 Hz at $\tau = 0.0$ and 0.125, as shown in Fig. 5. However, during the following time period from $\tau = 0.125$ to 0.25, the Nusselt number increases with increasing frequency due to an increase in flow acceleration, especially in the wake region.

The space-averaged Nusselt number (Nu_s) is calculated from Nu_θ using equation (7). This space-averaged Nusselt number is shown in Fig. 6(a) for Re_1 of 6.3, 15.2, 31.5, 62.9, 94.4 and $Re_0 = 0$ (no steady flow) for $S = 0.0067$–0.1 ($f = 1000$ Hz) as a function of dimensionless time. The normalized acoustic velocity (U/U_1) is shown in Fig. 6(b). In this Strouhal number range, the space-averaged Nusselt number exhibits an initial transient state and reaches the steady periodic state after about four or five cycles. This quasi-steady space-averaged Nusselt number is shown in Fig. 7 over one cycle after the steady periodic state has been

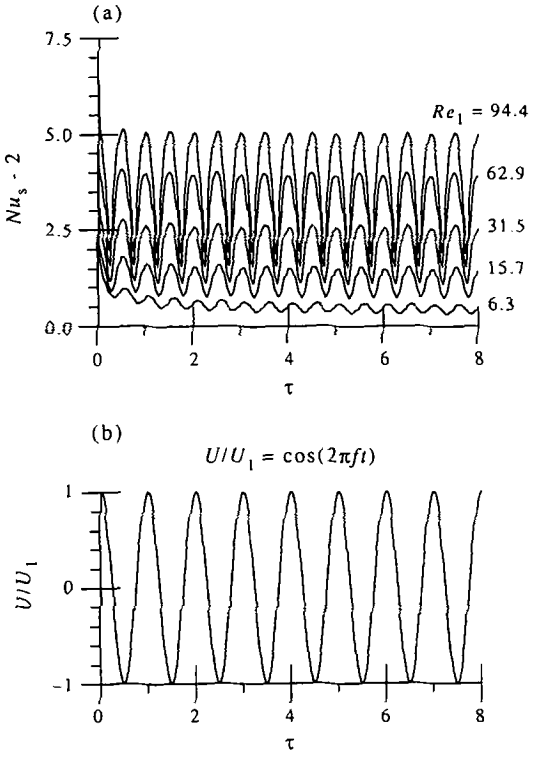

FIG. 6. (a) Space-averaged Nusselt number as a function of τ for $S = 0.0067$–0.1 for acoustic Reynolds numbers in the range 6.3–94.4 (SPL = 143–167 dB) and (b) the applied acoustic field with no steady flow.

reached. One can observe the cyclic behavior of Nu_s from Figs. 6 and 7. With increasing acoustic Reynolds number (increasing U_1) an increase in the mean value and amplitude of oscillation of Nu_s is observed.

The frequency effects on the quasi-steady space-averaged Nusselt number are shown in Fig. 8 at Re_1 of 15.7, 31.5, 62.9, 94.4 and $Re_0 = 0$ (no steady flow) for 50, 1000 and 2000 Hz. As already mentioned, at a low acoustic Reynolds number of 15.7, the characteristic time scale of heat transfer $t_{ch,T}$ is smaller than

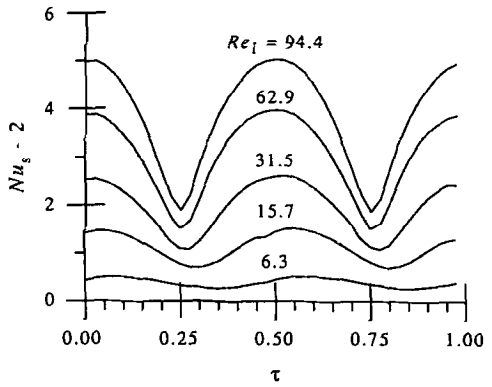

FIG. 7. Quasi-steady space-averaged Nusselt number during a cycle: $S = 0.0067$–0.1, $Re_0 = 0.0$ (no steady flow), $Re_1 = 6.3$–94.4 (SPL = 143–167 dB).

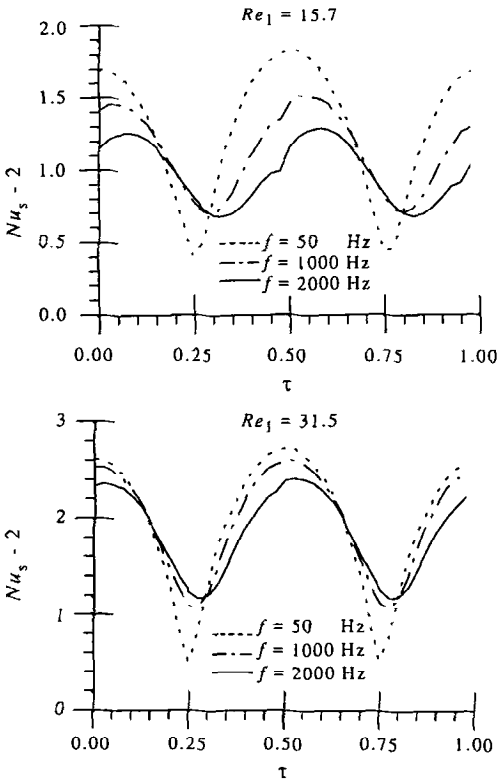

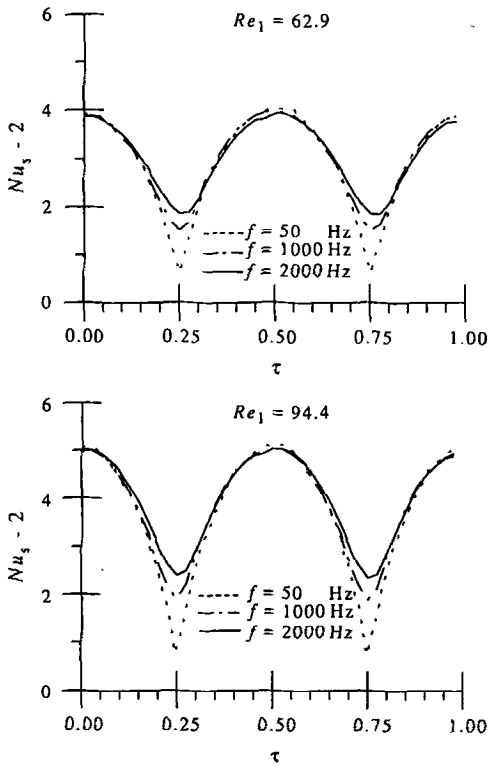

FIG. 8. Quasi-steady space-averaged Nusselt number for frequencies of 50, 1000 and 2000 Hz: $S = 0.0067$–0.1, $Re_0 = 0.0$ (no steady flow), $Re_1 = 6.3$–94.4 (SPL = 143–167 dB).

that of the oscillating flow $t_{ch,f}$ at 50 Hz, whereas $t_{ch,T}$ is larger than $t_{ch,f}$ at 2000 Hz. Therefore, the phase lag between the acoustic field and the thermal boundary layer increases as the frequency increases. This results in a decrease in the peak values of the space-averaged Nusselt number, Nu_s-2, corresponding to the high values of the oscillating velocity U, as shown in Fig. 8. The two high peak values of Nu_s-2 at 50 Hz are 1.702 and 1.825 at $\tau = 0.0$ and 0.5, respectively. When the velocity U is zero, the two low peak values of Nu_s-2 at 50 Hz are 0.415 and 0.439 at $\tau = 0.25$ and 0.75. When the frequency is increased to 2000 Hz, the two low peak values of Nu_s-2 are increased to 0.678 at $\tau = 0.325$ and to 0.679 at $\tau = 0.825$. The difference in time at which the peak values happen at different frequencies indicates the phase lag between the oscillating flow and the thermal boundary layer. These low peak values are higher than zero, which would be expected if $U_0 = 0$ for steady flow. Even though the oscillating velocity becomes zero some time, Nu_s-2 is not zero due to the phase lag between the acoustic field and the thermal boundary layer, and also due to the flow separation caused by flow acceleration at high frequency. The secondary effect is the acoustic streaming induced by the acoustic field as shown in refs. [17, 18].

When the acoustic Reynolds number Re_1 is increased to 94.4, $t_{ch,T}$ is smaller than $t_{ch,f}$ at both 50 Hz and 2000 Hz. As shown in Fig. 8, the two high peak values of Nu_s-2 at 50 Hz are 5.090 and 5.113 at $\tau = 0.025$ and 0.525, whereas those at 2000 Hz are 5.017 and 5.040 at $\tau = 0.025$ and 0.525. Therefore, the peak values of Nu_s-2 at 2000 Hz are almost the same as those at 50 Hz and they occur at the same values of τ. The two low peak values of Nu_s-2 corresponding to the zero value of the oscillating velocity U are 0.7526 and 0.7367 at $\tau = 0.25$ and 0.75 for 50 Hz. However, when the frequency is increased to 2000 Hz, the two low peak values of Nu_s-2 increase to 2.379 and 2.340 at $\tau = 0.25$ and 0.75. The flow separation as a result of high flow acceleration at 2000 Hz is responsible for the increase in the two low peak values of Nu_s-2 compared to those at 50 Hz, since there is no phase lag in this case.

Using equation (9), the space- and time-averaged Nusselt number, Nu_t-2 (Fig. 9), is obtained from the space-averaged Nusselt number, Nu_s-2 (Fig. 8). The dotted line in Fig. 9 is obtained from the following equation:

$$Nu_t-2 = 0.41954Re_1^{1/2}\,Pr^{1/3}. \tag{11}$$

This equation can be derived by introducing $U = U_1\cos(2\pi\tau)$ in place of U_0 in Re_0 of the correlation of Ranz and Marshall [11] as shown by Larsen and Jensen [5] and taking the time mean value over one period of oscillation. Similarly, the solid line is based on the correlation of Sayegh and Gauvin [13] for air, and the equation of which is:

$$Nu_t-2 = 0.272Re_1^{0.578}. \tag{12}$$

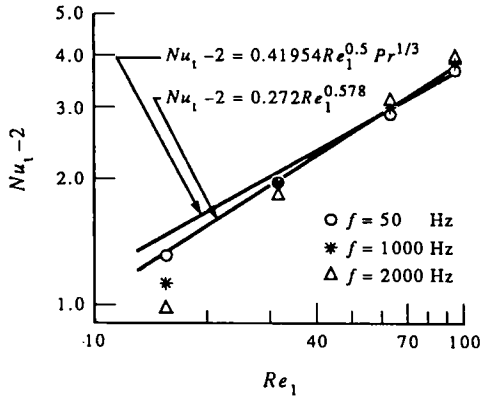

FIG. 9. Space- and time-averaged Nusselt number as a function of acoustic Reynolds number (no steady flow).

These space- and time-averaged Nusselt numbers given in equations (11) and (12) correspond to the limiting case of $t_{ch,f} \gg t_{ch,T}$. This means that there are no time delays between the oscillating flow and the thermal boundary layer response. As shown in Fig. 9, the equation (12) represents well the values of Nu_t-2 obtained at 50 Hz compared to those at 1000 and 2000 Hz. This indicates that, as the frequency gets smaller, the time constant of the external flow increases and the thermal boundary layer can respond quickly to the acoustic field.

As already mentioned, $t_{ch,T}$ at 50 Hz is smaller than $t_{ch,f}$ but $t_{ch,T}$ at 2000 Hz is larger than $t_{ch,f}$ for the acoustic Reynolds number of 15.7. This difference in the time scales between $t_{ch,f}$ and $t_{ch,T}$ results in the two high peak values of Nu_s-2 at 2000 Hz being less than that at 50 Hz and the two low peak values of Nu_s-2 at 2000 Hz being higher than that at 50 Hz, with a phase lag. The thermal boundary layer thickness δ_T gets thinner with increasing Re_1 and as a result $t_{ch,T}$ becomes smaller than $t_{ch,f}$ both for low and high frequencies. Therefore, the phase lag between the response and the acoustic field is reduced with increasing acoustic Reynolds number. The differences in the two high peak values of Nu_s-2 for the low and high frequencies are very small. With increasing Re_1, the flow acceleration at the high frequency leads to a larger separated flow region and makes an important contribution to the increase in the two low peak values of Nu_s-2 which are higher than the values at 50 Hz. Therefore, an increase in the values of Nu_t is observed with increasing frequency at an acoustic Reynolds number of around 100 and Nu_t at 2000 Hz is 4.0% higher than that at 50 Hz for the acoustic Reynolds number of 94.4, as shown in Fig. 9. A decrease is observed with increasing frequency at an acoustic Reynolds number of 10 and Nu_t at 2000 Hz is 9.4% lower than that at 50 Hz for the acoustic Reynolds number of 15.7.

SUMMARY AND CONCLUSIONS

The axisymmetric and laminar conservation equations for mass, momentum and energy for flow around a single spherical particle in the presence of an acoustic field are solved numerically with different values of acoustic Reynolds number and Strouhal number. The present simulation results compare well with the previously published results for the separation angle and the Nusselt number in the steady Reynolds number range of 10 to 100 without a superposed oscillating velocity ($Re_1 = 0$).

In the case of an oscillating flow around a spherical particle without steady velocity component, the velocity and temperature fields reach the steady periodic state after four or five cycles for low Strouhal numbers ($S = 0.00033$–0.08). The following are the major findings of the present studies:

(1) The values of Nusselt and Sherwood numbers depend on the characteristic time scale of the imposed oscillating flow and the boundary layer over the particle. The characteristic time scale for heat transfer ($t_{ch,T}$) at 50 Hz is smaller than that of the imposed oscillating flow ($t_{ch,f}$). Therefore, the time delay between the oscillating flow and the thermal boundary layer is very small. Thus, the correlation obtained by the quasi-steady analysis represents well the space- and time-averaged Nusselt number.

(2) At the acoustic Reynolds number of 15.7, the space- and time-averaged Nusselt number (Nu_t) at 2000 Hz is about 9.4% lower than that at 50 Hz whereas, at the acoustic Reynolds number of 94.4, Nu_t at 2000 Hz is about 4.2% higher than that at 50 Hz, due to the combined effects of the differences in the time scales and of the flow separation caused by the flow acceleration.

(3) The space- and time-averaged Nusselt number (Nu_t) is about 2.9 times higher than the value obtained when no acoustic field is present at an acoustic Reynolds number around 100.

(4) Increases in the Nusselt number are more significant for larger acoustic velocities, which correspond to the case of pulverized coal combustion and the later stages of coal–water slurry fuel combustion, under high intensity acoustic fields.

Acknowledgements—This work was supported by the U.S. Department of Energy, Morgantown Energy Technology Center, under contract DE-RA21-86MC23257.

REFERENCES

1. R. C. Marthelli and L. M. K. Boelter, The effect of vibration on heat transfer by free convection from a horizontal cylinder, *Proc. 5th Int. Congress of Applied Mechanics*, pp. 578–584 (1939).
2. C. B. Baxi and A. Ramachandran, Effect of vibration on heat transfer from spheres, *Trans. ASME, J. Heat Transfer* 337–344 (August 1969).
3. Y. Mori, M. Imabayashi, K. Hijikata and Y. Yoshida, Unsteady heat and mass transfer from spheres, *Int. J. Heat Mass Transfer* **12**, 571–585 (1969).
4. H. Gibert and H. Angelino, Transferts de matiere entre une sphere soumise a des vibrations et un liquide en mouvement, *Int. J. Heat Mass Transfer* **17**, 625–632 (1974).
5. P. S. Larsen and J. W. Jensen, Evaporation rates of drops in forced convection with superposed transverse sound field, *Int. J. Heat Mass Transfer* **21**, 511–517 (1978).
6. S. A. Rawson, An experimental investigation of the influence of high intensity acoustics on heat and mass transfer rates from spheres as related to coal–water slurry fuel combustion enhancement, M.S. Thesis, The Pennsylvania State University, Pennsylvania (1988).
7. S. V. Patankar, *Numerical Heat Transfer and Fluid Flow* (1st Edn). Hemisphere, Washington D.C. (1980).
8. F. P. Incropera and D. P. Dewitt, *Fundamentals of Heat and Mass Transfer* (2nd Edn), p. 284. Wiley, New York (1985).
9. J. P. Van Doormaal and G. D. Raithby, Enhancement of the SIMPLE method for predicting incompressible fluid flow, *Numer. Heat Transfer* **7**, 147–163 (1982).
10. R. Clift, J. R. Grace and M. E. Weber, *Bubbles, Drops, and Particles* (1st Edn), p. 103. Academic Press, New York (1978).
11. W. E. Ranz and W. R. Marshall, Evaporation from drops, *Chem. Engng Prog.* **48**, 141–146, 173–180 (1952).
12. T. Yuge, Experiments on heat transfer from spheres including combined natural and forced convection, *Trans. ASME, J. Heat Transfer, Series C* **82**, 214–220 (1960).
13. N. N. Sayegh and W. H. Gauvin, Numerical analysis of variable property heat transfer to a single sphere in high temperature surroundings, *A.I.Ch.E. Jl* **25**(3), 522–534 (1979).
14. K. Wong, S. Lee and C. Chen, Finite element solution of laminar combined convection from a sphere, *J. Heat Transfer* **108**, 860–865 (1986).
15. M. Y. Ha, A theoretical study of augmentation of particle combustion via acoustic enhancement of heat and mass transfer, Ph.D. Thesis, The Pennsylvania State University, Pennsylvania (1990).
16. W. F. Tseng and S. P. Lin, Transient heat transfer from a wire in a violently fluctuating environment, *Int. J. Heat Mass Transfer* **26**, 1695–1765 (1983).
17. J. M. Andres and U. Ingard, Acoustic streaming at high Reynolds number, *The Journal of the Acoustical Society of America* **25**(5), 928–932 (September 1953).
18. J. M. Andres and U. Ingard, Acoustic streaming at low Reynolds number, *The Journal of the Acoustical Society of America* **25**(5), 932–938 (September 1953).